First Year Report

Troy Vine, University College London

4th June 2004

Abstract

An investigation into gamma jet events in proton anti-proton collisions at a centre of mass energy $\sqrt{s} = 1.96$ *TeV using the* $\mathrm{K}_{\perp}$ *jet clustering algorithm. Differences are found between events simulated using the* HERWIG *and* PYTHIA *event generators. In particular a 12% shift is observed between the two in the mean of the ratio of the leading jet transverse momentum to that of the hard photon. Half of this can be accounted for by the 8% shift due to initial state radiation in quark initiated jets.*

1 Introduction

The last century has seen the description and understanding of the Universe undergo a radical paradigm shift. The thinking of Descartes, in the 16 Century, had left a fully deterministic scientific conception where every outcome was dictated by its cause. Investigation of the world on smaller length scales found that concepts form our everyday experience of the world cannot be simply carried over to the sub-atomic domain. A new conception was needed for a satisfactory explanation of black-body radiation and the Photoelectric effect. This lead to the theory of Quantum Mechanics. The most basic scientific assumptions of the world had been brought into question and radically altered. Physicists today generally use the Copenhagen Interpretation of Quantum mechanics to understand what the mathematics and the experiments say about the reality of what is happening. This philosophical view is based on a practical interpretation and leaves room for a deeper understanding of the nature of reality. One of the great strengths of Quantum Mechanics is its enormous predictive power and wide domain of application.

1.1 The Standard Model

One of the many fields of physics to enjoy the renaissance brought about by Quantum mechanics is High Energy Physics. This is an experimental science investigating the elementary building blocks of nature and their interactions. One method currently employed is colliding high energy particles in a detector. The theoretical understanding of experimental results has led to the development of Standard Model which describes the basic constituents of matter as local quantum fields which may be associated with a particle. The four fundamental forces (strong, electromagnetic, weak and gravitational) are understood as the momentum transfer of exchanged gauge bosons. A particle carrying an electric charge will interact via a massless gauge field called a photon. Quarks come in three charges or 'colours' and can only be observed in colourless combinations. Quarks interact via eight massless gluons and are described by Quantum ChromoDynamics (QCD). Unlike photons, gluons are self coupling and QCD interactions will therefore look very different to electromagnetic interactions described by Quantum Electrodynamics(QED). The strong coupling constant α_S is larger than that of QED and strong interactions will dominate at short range and confine quark combinations inside composite particles called hadrons. The weak force gauge bosons are the massive $W^{\pm}$ and Z^0. Gravitational effects are negligible on the scales of particle physics and there is no quantum theory of gravity in the Standard Model.

Due to energy and momentum conservation, which arise from demanding invariance of a physical system under global coordinate transformations, these exchanged gauge bosons are not real and $E^2 + P^2 - m^2$ will be non-zero contrary to real or on-mass-shell particles. This arises from Heisenberg's Uncertainty Principle which permits an energy fluctuation such that the product of the fluctuation and the time over which it occurs is within a certain limit.

In the Standard Model fermions (quarks and leptons) are point-like, and thus elementary, and exist in three generations of pairs. Also, all particles have antiparticles. The observed property of mass is described by the interaction of fermions with the Higgs field [1]. The associated field quanta, the Higgs boson, is an observable particle which is, as yet, undetected. If the Higgs boson were shown not to exist then another theory beyond the Standard Model is required, opening the way to new physics and a new paradigm to understand the fundamental structure of the universe.

1.2 Top Quark Mass

The third generation of quarks was discovered by the observation of the bottom (b) quark in 1977 at the Fermi National Accelerator Laboratory (FNAL). The verification of the existence of its partner, the top (t) quark, at FNAL in 1994 was vital for the validity of the Standard Model. The top mass was found to be $m_t = 174.3 \pm 5.1$ GeV [2], 35 times greater than the bottom quark mass. Due to its large value, m_t sets the strength of quark loop corrections in tree-level diagrams and is proportionally the most important parameter in the precision of Standard Model calculations.

The W mass (M_W) has loop corrections proportional to m_t^2 and $ln(M_H)$ thus providing an indirect way to measure the Higgs mass. The Z^0 mass has been calculated to high precision at the Electron Positron Collider (LEP), but the error on m_t and M_W is still relatively large and constrains the Higgs mass to a certain region. From run I data (1992-1995) at Fermilab

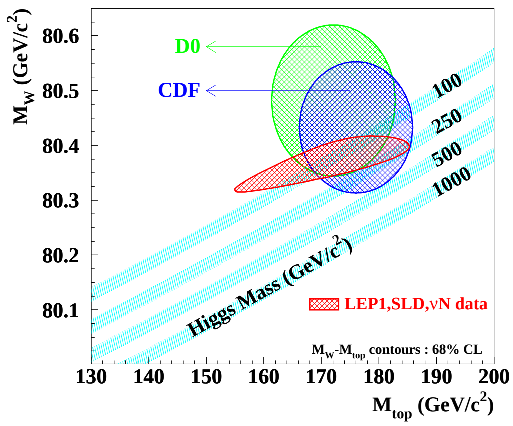

Figure 1:

the error on M_W has been reduced to ± 60 MeV [3], and the precision fit of the Higgs mass is currently limited by the error on m_t and M_W. The statistical error on m_t will be greatly reduced by the increase in luminosity of Run II. Fig 1 shows the Any quark or gluon from the $p\overline{p}$ collision will result in a jet of hadrons, and the largest contribution to the systematic error on the top mass is currently dominated by the calibration of the energy scale of this jet.

This report outlines an ongoing investigation into jet properties which will allow a more precise method to find the kinematics of the initiating quark or gluon from that of the jet and ultimately give a tighter constraint on the Standard Model Higgs mass.

1.3 Units and Nomenclature

Throughout this report natural units have been used, $\hbar = c = 1$. Mass, momentum and energy can therefore be expressed in giga electronvolts (GeV). Conversion to SI units can be made using the appropriate factors of $\hbar = 6.582 \times 10^{25}$ GeVs and $c = 3 \times 10^8$ ms^{-1}. Also, as the physics of a quark and its corresponding antiquark is identical in strong interactions, the term quark will be taken to include antiquark.

2 Experimental Apparatus

Sufficiently energetic collided particles will create virtual bosons which may decay, via many intermediate stages, into stable particles. This provides a method of investigating the properties of the different bosons and their decays. Although $p\overline{p}$ collisions do not produce the clean environment obtained by electron-positron collisions, much higher energies can be obtained and the huge increase in computer processing provides sophisticated triggering and analysis that

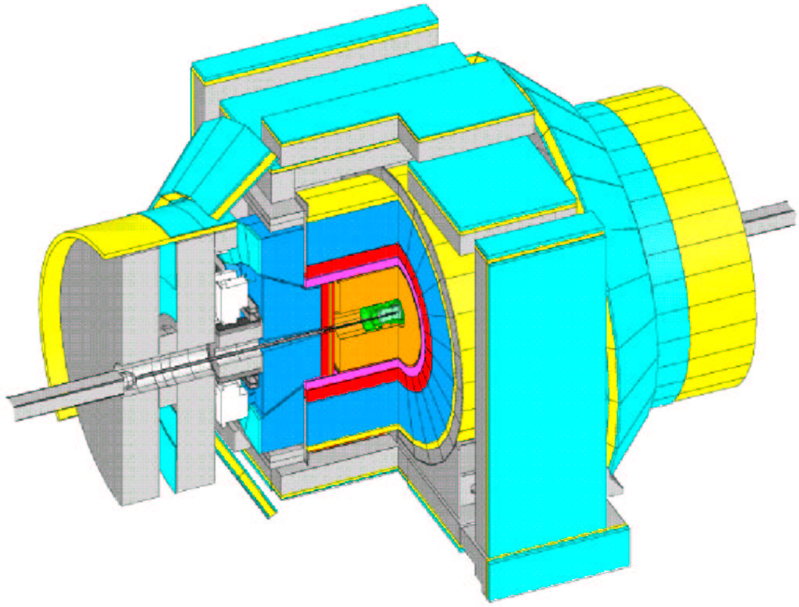

Figure 2: *The CDF Detector.*

can reduce the background contamination (fake rate) and increases the resolution (acceptance efficiency).

Particles are accelerated in the Tevatron synchrotron accelerator and collided in the two detectors, CDF and DØ. After Run I the Tevatron has been upgraded. The centre of mass energy has been increased from 1.8 TeV to 1.96 TeV and the instantaneous luminosity has increased from $1 \times 10^{31} cm^{-2}s^{-1}$ to $5 \times 10^{31} cm^{-2}s^{-1}$. Higher luminosities were originally expected for run II but the reduction of the current proton/antiproton bunch spacing of 396ns to 132ns has not been possible.

Nevertheless, a huge increase in integrated luminosity will allow a big reduction in the statistical error on the top mass and the W boson.

2.1 CDF Detector

The Collider Detector at Fermilab (CDF), shown in Fig. 2, is an azimuthally symmetric, general purpose detector [4]. It was upgraded along with the Tevatron and optimised for the higher luminosities of run II. It has a central barrel region and two end-cap (plug) regions. Tracking in the central region $|\eta| \leq 1$ is done by the Silicon Vertex Detector (SVX) surrounded by a wire drift chamber, the Central Outer Tracker (COT), between which is sandwiched the Intermediate Silicon Layer (ISL). This is all inside a 1.4 T magnetic field generated by a superconducting solenoidal magnet. Outside this is the calorimetry system: In the central region is Central Electromagnetic calorimeter (CEM) and the Central Hadronic Calorimeter(CHA). The plug consists of the Plug Electromagnetic Calorimeter (PEM) and the Plug Hadronic calorimeter (PHA). The gap between the central and plug region is covered by the End-Wall Hadronic Calorimeter (WHA). Muons will deposit very little energy in the calorimeters so muon trackers are installed around them. The central region has the Central Muon detector (CMU) surrounded by the Central Muon upgrade detector (CMP). Around the plug region is the Barrel Muon Detector (BMU) and between that and the central muon detectors is the Central Muon Extension (CMX) detector.

The collision rate is much higher than the speed at which data can be recorded therefore fast, real time triggering is required to select interesting events and reject soft, minimum bias events. There are three levels of triggers the event must pass before being written to tape.

3 Underlying Physics

Quantum mechanics describes physical processes in terms of probability distributions. Due to this underlying randomness, and Heisenberg's Uncertainty Principle, the comparison of experimental data with theory will show fluctuations which may be large, even if the theory is correct and the data acquired with precision. Also, several of the physical processes in a high energy interaction cannot be derived from first principles and therefore cannot be compared directly with theory. Thus to predict and understand the results, the physical event needs to be simulated.

3.1 Event Subprocesses

The proton is a composite object made up of confined partons (quarks and gluons). In a hard $p\overline{p}$ collision some of the partons interact strongly and the proton structure is broken. The event may be described in terms of the leading order diagrams e.g. $q\overline{q} \rightarrow g\gamma$ although many further interactions take place. These interactions can be categorised into the following subprocesses:

1. **Hard Subprocess**
   A hard interaction is a high transverse momentum ($\mathrm{P}_{\perp}$) boson exchange between a parton from each of the incoming hadrons, and produce two outgoing partons carrying some fraction of the total beam energy. High momentum transfers are described well by perturbative QCD and the hard subprocess can be calculated exactly from this theory. As QCD cannot yet predict the proton parton distribution from first principles, the parton distribution function (PDF) derived from parameterisation of experimental data is used.

2. **Initial State Radiation**
   Incoming partons can radiate gluons and, if they carry a charge, photons. For the partons carrying a large fraction of the total proton momentum, this radiation will contribute significantly to the overall event topology. Radiated gluons will hadronize.

3. **Final State Radiation**
   Partons after the hard subprocess can radiate as before in ISR.

4. **Hadronization**
   Outgoing and radiated partons will initiate a shower and produce a colourless collection of hadrons, leptons and photons. The structure of this process is given by the branching ratio of the QED ($e \to e\gamma$, $q \to q\gamma$) and QCD ($q \to qg$, $g \to gg$, $g \to q\overline{q}$) processes. Due to a large α_S, QCD radiation is very prolific and will dominate the shower. This process cannot be described from first principles and models have to be used.

5. **Underlying Soft Event**
   The underlying event is the contribution due to spectator parton interactions, and for this discussion the underlaying soft (low $P_\perp$) event is taken to refer to a contribution similar to minimum bias (non-single diffractive) event [5], which is dominated by soft interactions.

Categorising the whole event into the above subprocesses is useful for event simulation but somewhat arbitrary. A gluon radiated after the hard subprocess could fall into the ISR or Hadronization category, for instance, but the mathematical models used to simulate these two processes are very different.

3.2 Jets

The parton showers described in section 3.1 can be described in terms of jet characteristics. Qualitatively a jet is a collection of hadrons, photons and leptons confined to a certain angular region. To find a quantitative relation between the jet and the initiating parton a quantitative definition of a jet is required. There are two main types of jet definitions used in experimental physics:

1. **Cone Algorithms**
   Cone algorithms maximise the amount of energy deposited in a cone. While this provides a practical definition, the current understanding of perturbative QCD suggests that jets are not a collection of hadrons confined to cones of fixed angles.

2. **Clustering Algorithms**
   Clustering algorithms assign particles to jets based on their angle and their energy. Thus

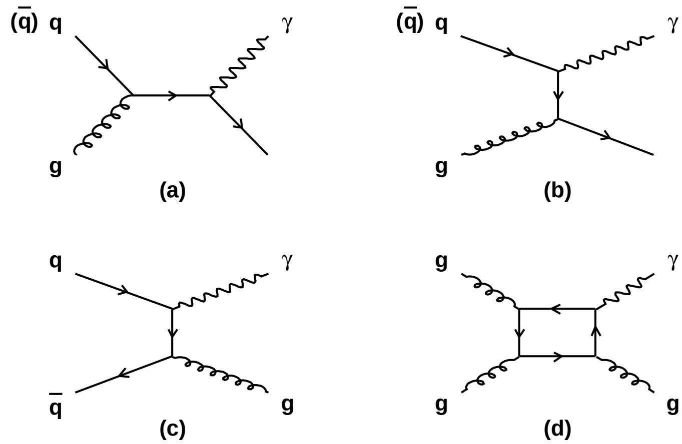

Figure 3: *The four leading order Feynman Diagrams for gamma jet events: (a, b)* $q\overline{q} \rightarrow g\gamma$*, (c)* $qg \rightarrow q\gamma$ *and (d)* $gg \rightarrow g\gamma$*.*

a soft hadron will be included in the nearest jet according to an energy-angle resolution parameter.

In this report the $\mathrm{K}_{\perp}$clustering algorithm is used with the ΔR scheme and the E recombination scheme (see [6] for the mathematical description of the different schemes).

3.3 Gamma-jet Events

The total cross section of $p\overline{p}$ collisions has a contribution from events where a hard photon and one or more jets are observed. In the centre of mass frame the hard photon recoils against the hard leading jet back-to-back. The distribution of the ratio of the leading jet $\mathrm{P}_{\perp}$ to that of the hard photon is used to calibrate the jet energy scale of the hadronic calorimeter. The relation of the $\mathrm{P}_{\perp}$ of a jet to that of its initiating parton is important for a quantative analysis and the error obtained in this will factor into the overall error of results obtained from studies involving jets. As the energy of the parton cannot be measured directly; this relation can only be found using event generators.

The Feynman Diagrams of the four leading order subprocesses for gamma jet events are shown in Fig. 3. Diagram (d) will be suppressed as it has four vertices instead of two.

4 Event Generators

Events are generated using Monte Carlo techniques. The many parameters in HERWIG and PYTHIA are constantly being tuned to fit current data and new data. For this investigation CTEC 5F PDF's are used [7].

4.1 PYTHIA

PYTHIA uses the Lund model [8] to simulate the hadronization subprocess. The outgoing and radiated partons will be colour connected to each other. These colour connections can be modelled as colour flux tubes which break by the process of pair production when they reach a certain $P_{\perp}$. This process will continue until on-mass-shell hadrons are obtained. The soft underlying event is modelled using soft multiple interactions between the incoming partons. These further colour connection are treated as above. The multiple interaction process is switched of by setting `MSTP(81)` to zero. ISR is switched off be setting `MSTP(61)` to zero.

4.2 HERWIG

HERWIG uses the cluster hadronization model [9]. This splits all glouns non-perturbatively into light quark-antiqaurk pairs. Thus by further radiation and decay a colourless cluster will result. The underlying soft event is modelled by superimposing a minimum-bias event onto the hard event. The underlying event is switched off by setting `Prsof` to zero in the `Underl_event` module and the ISR is removed by setting `Nospac` in the `Shower` module to 1.

5 Results and Conclusion

Comparisons are made between samples of events with and without ISR and the underlying soft event. For each sample more than 50,000 events were generated to limit statistical fluctuation. The plots in the right-hand column have ISR and the plots on the bottom row contain the underlying soft event

5.1 Errors

All plots are normalised to the number of events. The standard error formula has been used to calculate the error on the mean and for the error on the difference between the means ($\Delta mean$) the two mean error values are added in quadrature.

5.2 Selection

Due to the design of the CDF detector, a hard photon can be detected if it lies in the range $|\eta| \leq 1$ with a transverse momentum greater than 25 GeV. A simulation of the detector can be made on the generated events to enable comparison with experimental data. The same cuts are applied at the generator level, but with the minimum hard photon $P_\perp$ of 23 GeV to remove a bias due to discarding events where the hard photon $P_\perp$ could fluctuate up to the 25 GeV trigger level.

Diagram	HERWIG	PYTHIA
$qg \to q\gamma$ and $\overline{q}g \to \overline{q}\gamma$	85.6 ± 0.2	85.7 ± 0.2
$q\overline{q} \to g\gamma$	14.4 ± 0.1	14.3 ± 0.1
$gg \to g\gamma$	0.038 ± 0.005	0.031 ± 0.004

Table 1: *The percentage branching ratios of the leading order hard subprocesses.*

The branching ratios in Table 1 show that HERWIG and PYTHIA agree within the 1σ error quoted as is expected as same PDF's are used. The subprocess $gg \to g\gamma$ is clearly suppressed and events of this type are not included in this analysis as the statistics are too low. Classification of events as either quark initiated jets, with the hard subprocess (a) or (b) shown in Fig.1, or gluon initiated jets with hard subprocess (c).

5.3 Jet ϕ Distribution

From Fig. 4 the leading jet and the hard photon are back-to-back as expected (see section 3.3). The ISR can be seen to broaden the leading jet distribution in ϕ as the radiation will carry some $P_\perp$. The agreement between HERWIG and PYTHIA is good although HERWIG is a little broader with ISR.

It would be expected that jets from ISR are isotropically distributed in ϕ. The plots in Fig. 5 of the ϕ distribution of the second highest $P_\perp$ jets show that this is not the case. From the number of jets per event shown in Fig. 6 it is evident that the majority of next to leading jets are due to ISR and the difference between HERWIG and PYTHIA in the ϕ distribution of next to leading jets can be attributed to differences in how the ISR is modelled and the values of the parameters.

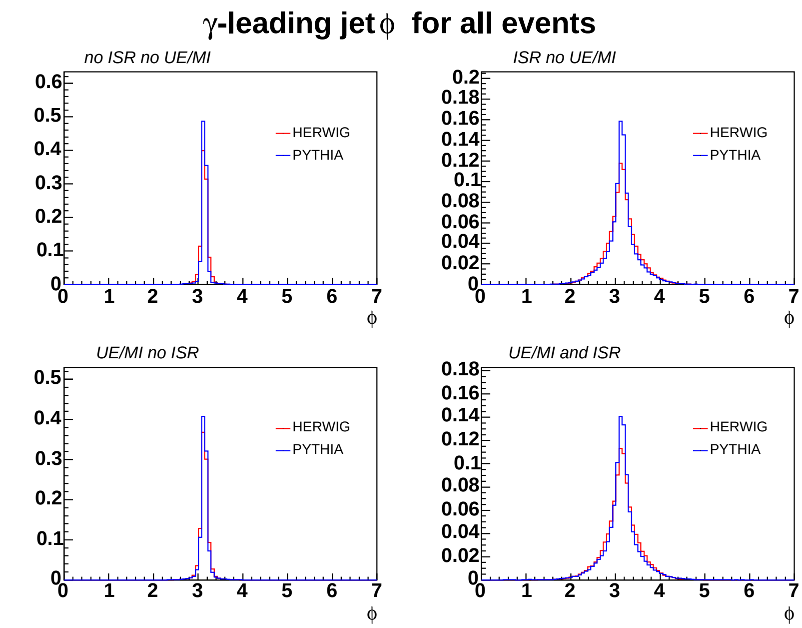

Figure 4: *The angle in ϕ between the leading jet and the hard photon for all hard subprocesses.*

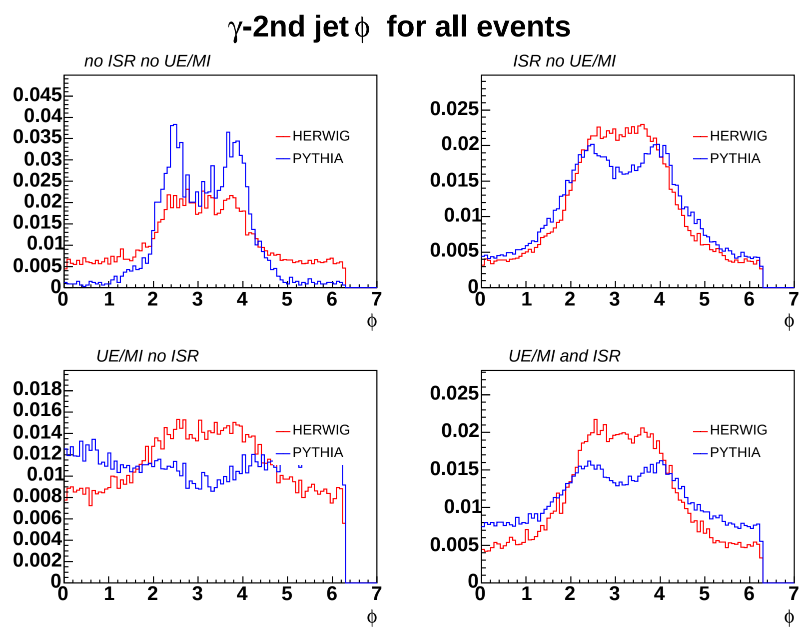

Figure 5: *The angle in ϕ between the next to leading jet and the hard photon for all hard subprocesses.*

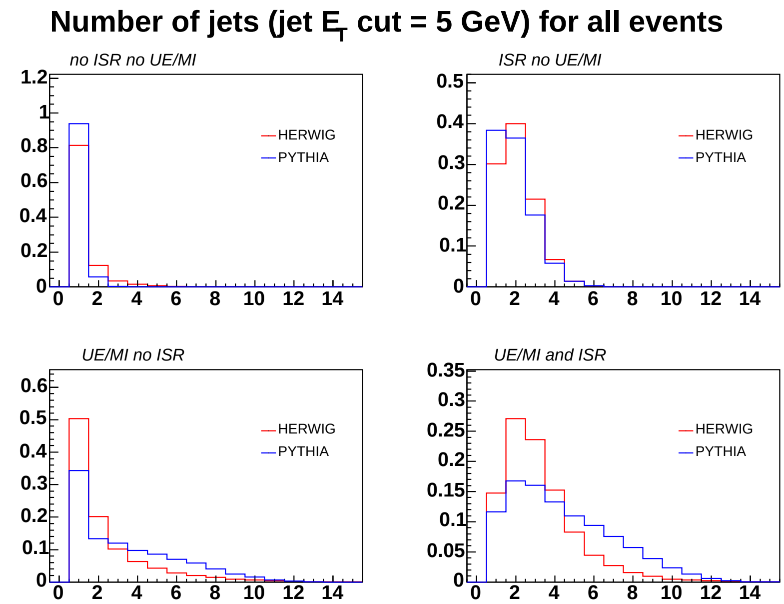

Figure 6: *The distributin of the number of jets per event.*

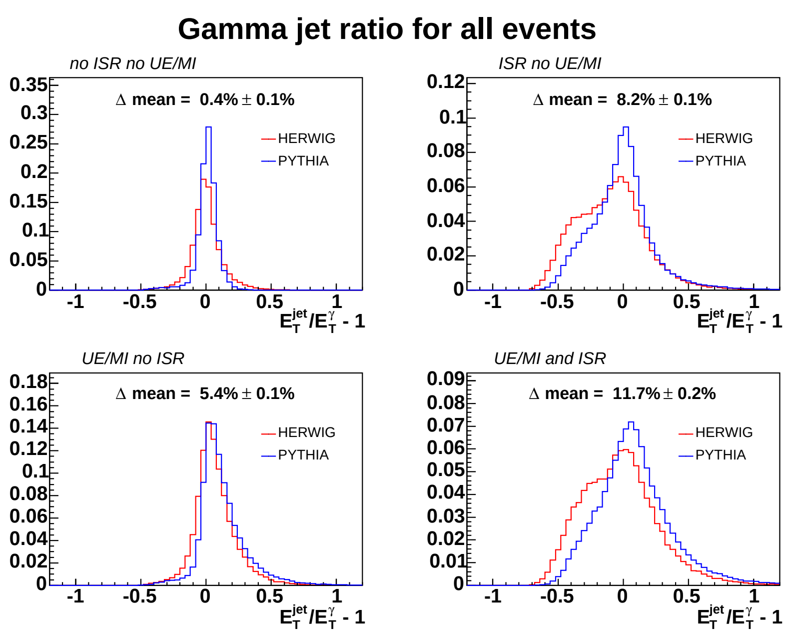

Figure 7: *Leading Jet* $P_\perp$ *to Hard Photon* $P_\perp$ *Ratio for all hard subprocesses.*

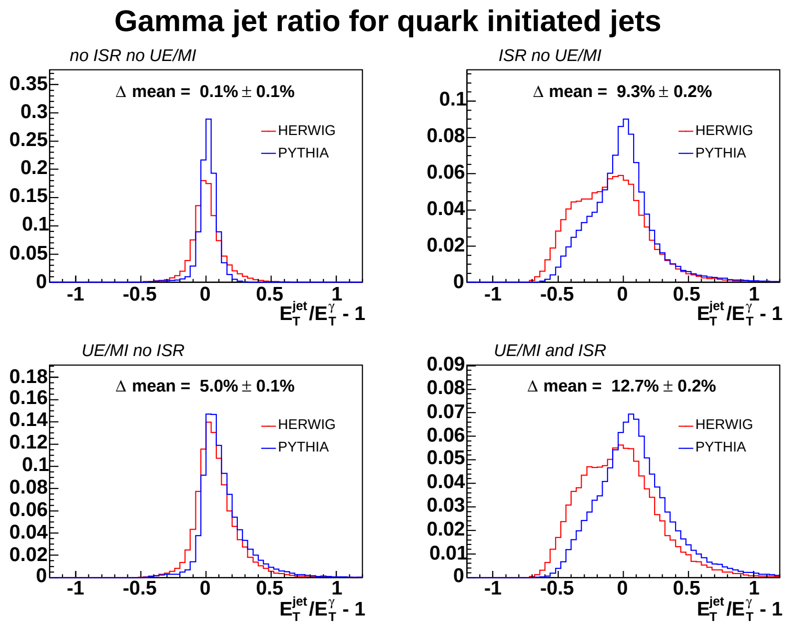

Figure 8: *Gamma-jet ratio for* $qg \to q\gamma$ *and* $\bar{q}g \to \bar{q}\gamma$ *events.*

5.4 Leading Jet $P_\perp$ to Hard Photon $P_\perp$ Ratio

The qualitative discussion in section 5.3 can be quantified by considering the difference in the mean of the leading jet $P_\perp$ to hard photon $P_\perp$ ratio. This is shown for all subprocesses in Fig. 7. With no underlying soft event the ISR gives a shift of 7.8%. Adding the underlying soft event without ISR gives a shift of 5%. Adding either of the two with the other already present reduces this shift indicating that they are not totally independent processes, which, in terms of the actual physics, they are not.

Fig. 8 and 9 show the the ratio of the leading jet $P_\perp$to that of the hard photon for gluon and quark initiated jets respectively. The ISR for model for gluon initiated jets behaves almost identical in HERWIG and PYTHIA for events with and without the underlying soft event. The biggest difference between HERWIG and PYTHIA, both in the mean and the shape, is the ISR from quark initiated jets. As this hard subprocess dominates gamma jet events, it has a big effect on the ratio for all events in Fig. 7.

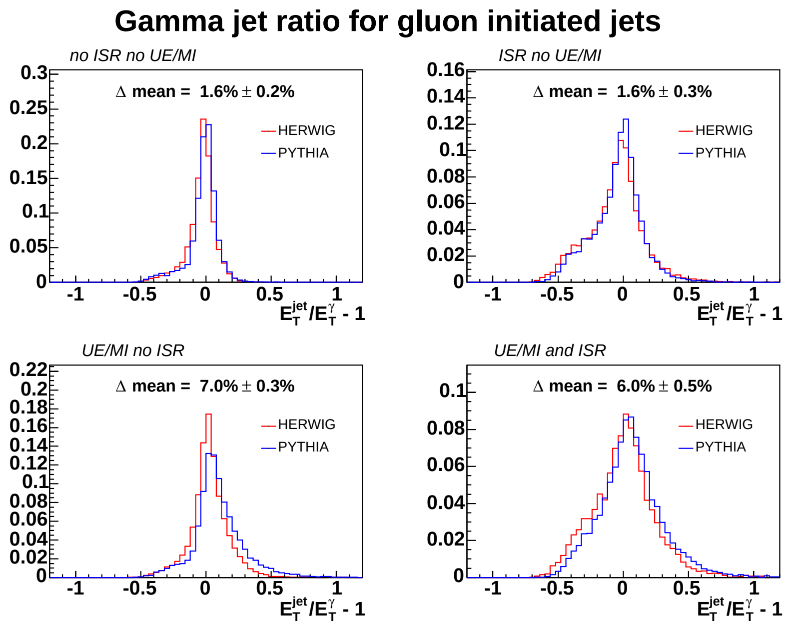

Figure 9: *Gamma-jet ratio for* $q\bar{q} \rightarrow g\gamma$*events.*

6 Conclusion

The principle discrepancy between HERWIG and PYTHIA in gamma jet events is the ISR radiation from quark initiated jets. This could be due to differences in how gluon radiated from gluons inside the proton is modelled. By including results from the hard subprocess $gg \rightarrow g\gamma$ this could be investigated.

The results presented in section 4 are only the beginning of the task of isolating the cause of the difference between HERWIG and PYTHIA and tuning them accordingly. Further, an agreement between the event generators is not very useful if it does not fit the data. Looking at quark and gluon initiated jets separately is useful to tune the generators but is limited to this as the data cannot be categorised in such a fashion. As mentioned in section 3.1 the classification of the whole event into subprocesses is arbitrary, and the models of the different processes do not necessarily reveal anything about the underlying physics of an event. In terms of actual physics there is only one process; the whole event, with an observer. To treat it as such is not yet possible but none-the-less a worthwhile cause.

References

[1] P. W. Higgs, Phys. Rev. Lett. **12**, 132 (1964).

[2] The CDF and DØ Collaborations, FERMILAB-TM-2084 (1999)

[3] The CDF and DØ Collaborations, FERMILAB-PUB-03/398-E (2003)

[4] CDF II Detector Technical Design Report (1996)

[5] The CDF Collaboration, FERMILAB-PUB-04/041-E (2004)

[6] J. M. Butterworth *et al*, Comput. Phys. Commun. **153/1**, 85 (2003)

[7] see http://www.phys.psu.edu/ cteq/

[8] T. Sjöstrand, Comput. Phys. Commun. **82**, 74 (1994).

[9] G. Marchesini *et al*, Comput. Phys. Commun. **67**, 465 (1991).